Since January 2020 Elsevier has created a COVID-19 resource centre with free information in English and Mandarin on the novel coronavirus COVID-19. The COVID-19 resource centre is hosted on Elsevier Connect, the company's public news and information website.

Biosensors and Bioelectronics 192 (2021) 113536

Contents lists available at ScienceDirect

Biosensors and Bioelectronics

journal homepage: www.elsevier.com/locate/bios

Point-of-need detection of pathogen-specific nucleic acid targets using magnetic particle spectroscopy

Enja Laureen Rösch [a], Jing Zhong [a], Aidin Lak [a], Zhe Liu [b], Markus Etzkorn [b], Meinhard Schilling [a], Frank Ludwig [a], Thilo Viereck [a], Birka Lalkens [c,*]

[a] Institute for Electrical Measurement Science and Fundamental Electrical Engineering and Laboratory for Emerging Nanometrology (LENA), TU Braunschweig, Hans-Sommer-Str. 66, Braunschweig, 38106, Germany
[b] Institute of Applied Physics, TU Braunschweig, Mendelssohnstraße 2, 38106, Braunschweig, Germany
[c] Institute of Semiconductor Technology and Laboratory for Emerging Nanometrology (LENA), TU Braunschweig, Langer Kamp 6a/b, 38106, Braunschweig, Germany

ARTICLE INFO

Keywords:
Magnetic particle spectroscopy
Point-of-need
Diagnostics
SARS-CoV-2
Magnetic nanoparticles

ABSTRACT

The ongoing COVID-19 pandemic stresses the need for widely available diagnostic tests for the presence of SARS-CoV-2 in individuals. Due to the limited availability of vaccines, diagnostic assays which are cheap, easy-to-use at the point-of-need, reliable and fast, are currently the only way to control the pandemic situation.

Here we present a diagnostic assay for the detection of pathogen-specific nucleic acids based on changes of the magnetic response of magnetic nanoparticles: The target-mediated hybridization of modified nanoparticles leads to an increase in the hydrodynamic radius. This resulting change in the magnetic behaviour in an ac magnetic field can be measured via magnetic particle spectroscopy (MPS), providing a viable tool for the accurate detection of target nucleic acids.

In this work we show that single stranded DNA can be detected in a concentration-dependent manner by these means. In addition to detecting synthetic DNA with an arbitrary sequence in a concentration down to 500 pM, we show that RNA and SARS-CoV-2-specific DNA as well as saliva as a sample medium can be used for an accurate assay. These proof-of-principle experiments show the potential of MPS based assays for the reliable and fast diagnostics of pathogens like SARS-CoV-2 in a point-of-need fashion without the need of complex sample preparation.

1. Introduction

The current pandemic situation caused by severe acute respiratory syndrome coronavirus 2 (SARS-CoV-2) urgently demonstrates the need for a fast and accurate diagnostic workflow: strong political measures like travel restrictions or lockdowns are based on the number of acutely infected people (Haug et al., 2020). While PCR-testing remains undoubtedly the gold standard for sensitive and accurate diagnosis (Kevadiya et al., 2021a,b), there is a need for alternative rapid testing approaches, bypassing supply and personnel shortfalls as well as enabling point-of-need testing for critical situations like for example contacts with vulnerable people (Islam and Iqbal, 2020; Morales-Narváez and Dincer, 2020).

Due to the large demand, in the last months, a plethora of methods for fast diagnostics of acute infections have been developed, testing either for genetic information from the virus or virus-specific proteins (Arnaout et al., 2020; Bhavesh D. Kevadiya et al., 2021a,b; Guglielmi, 2020; Oliveira et al., 2020; Ravi et al., 2020; Vandenberg et al., 2021).

RT-PCR-based techniques can detect down to single copies of the virus, being ultimately sensitive (Afzal, 2020; Park et al., 2020; Zhou et al., 2020). However, this comes at the cost of rather high prices, the demand of sample purification and well-equipped laboratories, hindering the usage at the point of need, as is increasingly necessary to stop the further spreading of the virus. To circumvent these problems, amongst others, promising CRISPR-based diagnostics tool are developed, allowing for the sensitive detection on mobile devices (Fozouni et al., 2020) .

In addition to nasopharyngeal swabs, saliva is now emerging as a viable tool for sample drawing (Azzi et al., 2020), making point-of-need-testing more accessible to untrained personnel in a pain-free matter. Recent studies indicate that also in saliva, high viral loads of viral nucleic acids can be detected. Depending on the stage of the infection, 10^4 to 10^8 copies per mL have been detected in saliva of

* Corresponding author.
E-mail address: b.lalkens@tu-braunschweig.de (B. Lalkens).

https://doi.org/10.1016/j.bios.2021.113536
Received 25 June 2021; Received in revised form 23 July 2021; Accepted 24 July 2021
Available online 27 July 2021

infected people (Zhu et al., 2020). For an effective point-of-need-testing, this rather high viral load shows that ultra-high sensitivity with detection of single molecules is not necessarily required for a fast identification of potentially infectious people.

Magnetic Particle Spectroscopy (MPS) can be a valuable, low-key addition to these diagnostic devices, as it is based on a simple measurement setup suitable for a rapid point-of-need application. In MPS, magnetic nanoparticles (MNPs) are exposed to a time-varying magnetic field. The applied field is strong enough to at least partially saturate the particles, generating a non-linear magnetization response, which is harvested by a differential pick-up coil and analyzed in Fourier-domain (Biederer et al., 2009; Wawrzik et al., 2012). The magnetic moments of MNPs tend to align with the applied fields through Néel and Brownian relaxation processes, which are countered by thermal energy k_BT (Draack et al., 2019b). For bioassays, especially the Brownian relaxation time constant τ_B is directly linked to physical conditions such as the viscosity η of the medium as well as the hydrodynamic volume V_H of the MNPs (Draack et al., 2019a).To this end, a change in hydrodynamic radius, caused by an analyte binding to the particles or MNP cluster formation, is reflected in a change in Brownian relaxation time and consequently in a reduction of higher harmonic components (assuming Brownian-dominated particles) in the observed spectrum. Advantages of this approach include the very limited sample processing necessity, the long-term stability of instrument and sample, the possibility to measure in opaque media, extremely short measurement times and the potential of quantification (Schrittwieser et al., 2016). Due to the ease of the measurement process, there are a number of application currently developed using MPS (Khurshid et al., 2017; Poller et al., 2016; Rauwerdink and Weaver, 2010; Tian et al., 2020; Wu et al. 2019, 2020a, 2020b; Zhong et al. 2021a, 2021b).

In this work, the sequence-specific hybridization process of single stranded nucleic acids is utilized to change the hydrodynamic radius of the MNPs in the presence of the target. A custom-built MPS setup is used to measure the MPS characteristics of functionalized MNPs within seconds. Due to the limited sample preparation, this allows for a fast and easy-to-use diagnostic assay. Since the hybridization is ubiquitous, we expect this method to be easily adaptable to new sequences and therefore also new infectious targets or related mutations, paving the way for the development of quantitative, rapid and cost-efficient point-of-need-assays.

2. Experimental

In this paper, Brownian-relaxation-dominated MNPs (Ahrentorp et al., 2015; Kahmann and Ludwig, 2020) are used to detect specific single-stranded (ss) target DNA. The MNPs used are Bionized Nano-Ferrite particles with a mean diameter of 80 nm (BNF80), coated with streptavidin, purchased from micromod Partikeltechnologie GmbH (Rostock, Germany). The BNF80 stock solution has an iron concentration of 5.5 mg/ml and a particle molar concentration of 20 nM. Throughout the experiments, the stock solution has been diluted to 2 nM.

Streptavidin-coated polystyrene (PS) beads with a diameter of 100 nm were purchased from micromod Partikeltechnologie GmbH. The stock solution has a concentration of 10 mg/ml and a molar concentration of 31.5 nM. Throughout the experiments, the stock solution has been diluted to 3.5 nM.

Biotinylated DNA oligonucleotides and single stranded target DNA were purchased from eurofins genomics GmbH (Ebersberg, Germany) in a concentration of 100 pmol/µl with HPSF-purification.

All other chemicals were purchased from Sigma-Aldrich, unless otherwise mentioned.

2.1. Particle functionalization

All samples were prepared with a total volume of 90 µl. For the functionalization of the MNPs and PS beads, a protocol based on published methods (Tian et al. 2018, 2020) was developed: 2 nM of streptavidin-coated BNF80 in 9 µl PBS buffer (phosphate buffered saline, 0.14 M NaCl, 2.7 mM KCl, 10 mM phosphate, pH 7.4) were incubated with 133.3 nM biotinylated DNA in 12 µl buffer solution, whereas 3.5 nM PS beads in 10 µl buffer were incubated with 244.4 nM biotinylated DNA in 22 µl buffer for 1 h at 27 °C. To eliminate nonspecific binding of streptavidin, 111.1 µM of free biotin in 10 µl buffer was added to the particle's solution and incubated at 27 °C for 1 h. In case washing was applied, particles were purified from the excess biotinylated DNA strands by amicon filtering (amicon ultra-0.5 mL, ultracel 100 K membrane, millipore) and three times washing with 1xTE buffer (0.1 M Tris-HCl, 10 mM EDTA, pH 7.4) containing 12 mM $MgCl_2$. Each time it was centrifuged for 5 min at 14000 rcf and 4 °C before flipping the amicon filter and placing in a new tube. By centrifugation for 5 min at 1000 rcf and 4 °C, the purified particles were extracted. The extraction process was repeated by adding 100 µl buffer solution to the remaining MNPs in the amicon filter and centrifuging again at 1000 rcf and 4 °C.

2.2. Target incubation

For crosslinking MNPs with PS beads, 2 nM MNPs and 3.5 nM PS beads were mixed in TE-buffer containing 50 mM $MgCl_2$ and 0.2 % tween20 and incubated with the appropriate concentration of target DNA at 27 °C for 2 h.

For the preparation of diluted samples, the MNPs and PS beads were diluted in 1 ml and 5 ml buffer solution resulting in a molar concentration of 180 pM and 36 pM for MNPs and 315 pM and 63 pM for the PS beads, respectively. The samples were incubated overnight with a target concentration of 5 nM, 1 nM and 0.5 pM. After incubation, the samples were up-concentrated using MS columns and the MiniMACS separator, purchased from Miltenyi Biotec (Bergisch Gladbach, Germany). First, the MS columns were rinsed with 500 µl buffer solution. Afterwards, the columns were placed in the MiniMACS separator, building up a magnetic field within the columns. The sample was filled in the columns and due to the strong magnetic field gradients in the column the MNPs remained in it. Subsequently, the column was removed from the magnetic separator and placed on a new collection tube. After pipetting 50 µl of buffer solution onto the column, the MNPs were flushed out with the supplied plunger. Due to the reduced sample volume, the molar concentration of MNPs is increased, generating a larger signal in the magnetic particle spectrometer. To obtain all MNPs in the columns, the wash-out step was repeated three times.

2.3. Preparation of RNA samples

To exclude RNase contaminations, all solutions except for TE buffer were incubated at 37 °C overnight with 0.1% diethyl pyrocarbonate (DEPC) and autoclaved at 121 °C for 15 min to eliminate residual DEPC. Fresh RNase-free TE-buffer was used. All surfaces were cleaned with RNase AWAY (Thermo Fisher).

The RNA target (biomers, Ulm, Germany) was kept on ice and otherwise incubated in the same way as the DNA target.

2.4. Saliva preparation

Freshly collected saliva was heat-inactivated by incubation at 95 °C for 30 min, then cooled down to 27 °C. Afterwards, 0.5 vol of concentrated TE buffer was added. 55.5 nM target DNA as well as 2 nM modified MNPs and 3.5 nM PS beads were added to the saliva solution.

2.5. Magnetic particle spectroscopy setup

MNP based biosensing utilizes the change of the Brownian relaxation time due to the change of the hydrodynamic diameter upon binding of biomolecules to the surface of the particles. The increase in the

hydrodynamic diameter of the MNPs results in a slower rotation of the particles in an ac magnetic field, leading to a change in the harmonic spectrum, e.g. a decrease in the third harmonic amplitude, which is investigated here.

In this paper, a custom built MPS setup was used. A Helmholtz coil generated the ac magnetic field for the MNP excitation. For the measurements of the MNP harmonics, a gradiometric pick-up coil was used, consisting of a detection coil and a balance coil. Further details regarding the setup can be found here (Zhong et al., 2018).

First, a blank measurement was performed. Afterwards, the MNP sample was exposed to an ac magnetic field with an amplitude of 10 mT with excitation frequencies f_0 varying from 180 Hz to 1418 Hz. Due to the magnetic response of the MNPs, a signal was induced into the pick-up coil. Subsequently, the blank measurement was subtracted from the measured signal for the calculation of the MNP signal. To eliminate the influence of the particles' concentration, the harmonic ratio of 3rd to 1st harmonic amplitudes, defining the i^{th} harmonic at frequency $i \times f_0$, was investigated. Upon target-mediated binding, the hydrodynamic radius of the MNPs increase and the 3rd harmonic amplitude strongly decreases, resulting in a lower harmonic ratio compared to a control sample without target present. Each measurement was repeated three times.

3. Results and discussion

3.1. Basic measurement principle

To detect the presence of specific single-stranded (ss) target DNA, magnetic nanoparticles as well as 100 nm diameter polystyrene (PS) beads were functionalized with ssDNA via biotin-streptavidin interactions as shown in Fig. 1A. To this end, streptavidin-coated MNPs and PS beads were incubated with biotinylated single-stranded (ss) 20T- and 20G-oligonucleotides, respectively. Since 20T and 20G show no complementarity, no interaction is expected. Only if a single-stranded target nucleic acid is added which is partially complementary to both the sequences of the MNPs and the PS beads (in this case a 20A20C sequence), oligonucleotide hybridization takes place, meaning in this case that the beads bind to the particles, thus showing an increase in hydrodynamic radius of the MNPs. A characterization of the particles and clusters by DLS and SEM imaging is presented in figure S1.

When a solution of MNPs is exposed to an ac magnetic field with an amplitude in the range of several milliTesla and a frequency f_0, the magnetization of the sample follows the particles' magnetization curve, which can be modelled by a Langevin function (Fig. 1B). The resulting MPS signal contains not only the fundamental frequency f_0, but also higher harmonics at frequencies $n \cdot f_0$. Unbound particles can freely rotate and align with the external field in a certain frequency range. Upon target-mediated binding of the PS beads, the hydrodynamic radius of the MNPs increases. Consequently, the particles' relaxation time increases, which causes a significant decrease in the higher odd

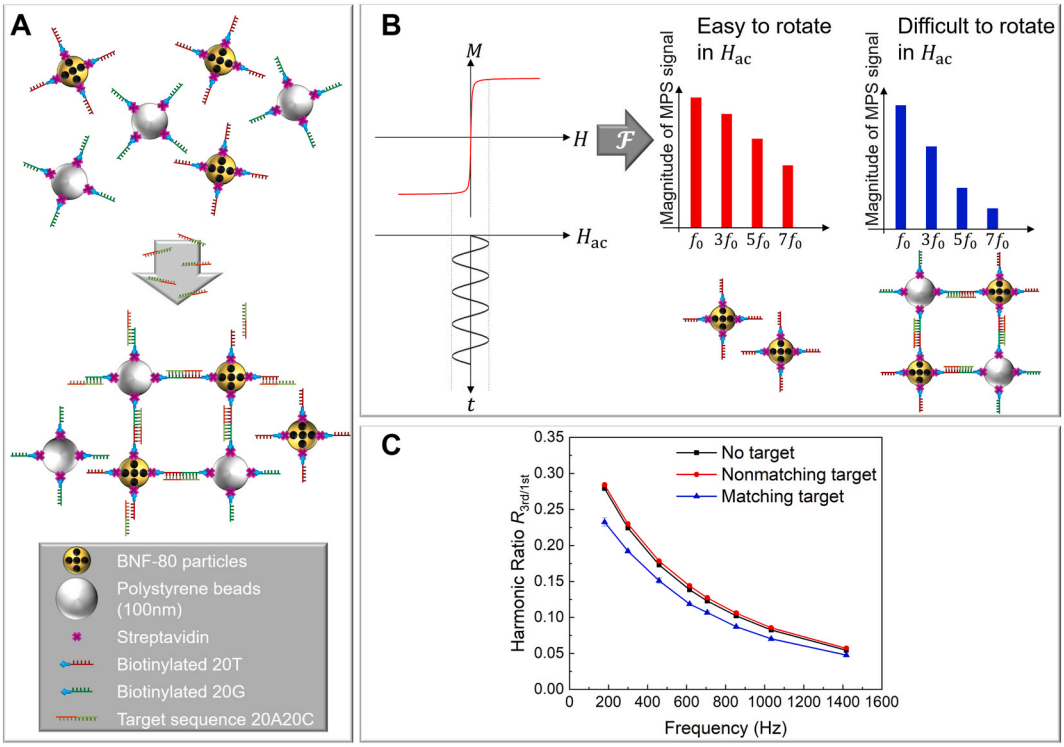

Fig. 1. Assay Principle. A: magnetic nanoparticles (gold) and polystyrene beads (silver) with streptavidin (purple) - modified surface are equipped with single-stranded DNA strands (red and green, respectively) with a specific sequence via biotin-streptavidin-binding. Upon addition of a single-stranded nucleic acid target (light-red/light-green), which is complementary to both the sequences on magnetic particles and polystyrene beads, crosslinking mediated by specific hybridization of the single-stranded nucleic acids between the particles takes place, yielding magnetic nanoparticles with an increased hydrodynamic radius. B: Applying a sinusoidal magnetic field (black) to a solution of nanoparticles results in reorientation of the nanoparticles which can be read out by measuring the magnetic response M of the nanoparticles. Depending on features like the hydrodynamic radius of the nanoparticles, the reorientation is slower (blue) or faster (red), leading to a change of the amplitudes of higher harmonics in the received signal. C: Exemplary spectrum of the ratio of received harmonics as a function of excitation frequencies for 80 nm BNF magnetic particles. When adding a non-matching target (red), no target-mediated crosslinking between the particles occurs, leading to a spectrum very similar to measurements of a solution of magnetic particles and polystyrene beads without any target (black). Upon addition of a matching target a shift to smaller ratios is observed, which is due to the increase of the hydrodynamic radius and therefore slower reorientation in the magnetic field by crosslinking of the particles (blue). (For interpretation of the references to color in this figure legend, the reader is referred to the Web version of this article.)

harmonics, as shown in Fig. 1B. By calculating the harmonic ratio, in this case 3rd to the 1st harmonic (which corresponds to the fundamental frequency), the influence of the particles' concentration is eliminated. A reference sample containing only modified MNPs and PS beads (Fig. 1C, black) shows a higher harmonic ratio for all measured frequencies than the same sample in presence of the target DNA (Fig. 1C, blue). If using a non-matching DNA oligonucleotide 20T20G as a target, no decrease in harmonic ratio is observed (Fig. 1C, red). Only in presence of the correct complementary target, a DNA-mediated binding of the PS beads to the MNPs occurs, which is detectable in a change in the MPS signal. The specificity is further demonstrated by additional experiments using other non-matching target sequences (Fig. S2). This shows that MPS measurements can be a valuable read-out for the presence of specific nucleic acids.

Eight different excitation frequencies of the magnetic field between 180 Hz and 1418 Hz with an amplitude of 10 mT were applied. For each sample, four measurements were taken at each frequency, with standard deviations added to the curve. The measurement time for the current MPS setup is approximately 2 s per frequency.

Free biotinylated oligonucleotides in solution (e.g. not bound to MNPs and PS beads) would interfere with the assay, since they would compete for target binding, leading to a reduction in binding of the PS beads to the MNPs and therefore to a less-pronounced change in the MPS signal. Therefore, a 1.25-fold excess of biotin binding sites on MNPs and PS beads to biotinylated oligonucleotides was used, minimizing the amount of unbound oligonucleotides in solution. To ensure stable cluster formation, ssDNA modifications on both MNPs and polystyrene beads had a length of 20 nucleotides each for stable hybridization.

The addition of modified PS beads to modified MNPs also accounts for a reduction of harmonic frequencies compared to the signal obtained by measuring the modified MNPs without PS beads (see Fig. S3). We account incomplete saturation of streptavidin and corresponding partial crosslinking of the beads to be responsible for that; an additional saturation with free biotin before mixing MNPs and PS beads can inhibit this crosslinking (compare Fig. S3). Furthermore, addition of 0.1% tween20 can further reduce unspecific crosslinking.

3.2. Target concentration dependency

In order to estimate the influence of the target concentration on the harmonic ratio, different amounts of target DNA were added to the sample. Fig. 2 shows the harmonic ratio for target concentrations between 0.5 nM and 50 nM. For increasing target concentration, a decrease of the harmonic ratio is observable. However, for 30 nM and 50 nM target concentration, this tendency is less pronounced. For quantification of these results, we introduce the relative change δ which is $\delta = (R_0 - R_c)/R_0$. δ corresponds to the target-binding mediated change in signal and is a measure for the sensitivity of the test. The bigger δ, the stronger the target-mediated effect on the MPS signal. Therefore, δ can be used to estimate the performance of the test under given parameters. For a prospective assay for the presence of target nucleic acid in the sample, δ can furthermore be used to define ranges for positive and negative test results. Fig. 2B shows δ at 459 Hz for different target concentrations: For concentrations of up to 10 nM, δ exhibits a linear dose-response relation. For higher concentrations >10 nM, a saturation effect is observed: Higher target concentrations do not lead to a further linear increase in δ, because binding sites on the MNPs as well as on the PS beads will eventually be saturated with single-stranded target, ultimately leading to a discontinuation of target-mediated crosslinking. For estimating the limit of detection of this approach, using the 3s-criterion (Armbruster and Pry, 2008) gives a limit of detection of 0.28 nM with a linear range up to 10 nM.

This shows that - within a concentration range up to 10 nM - the readout of the MPS signal is sensitive to the amount of DNA to be detected, allowing for an estimate of the target concentration in the sample.

Since there is no washing step after functionalizing both NPs and PS beads with biotin-functionalized DNA, we expect also free biotinylated ssDNA to be present in the sample. This free ssDNA will preferentially hybridize to the target DNA, decreasing the amount of target DNA for efficient hybridization of MNPs and PS beads and therefore effectively decreasing the sensitivity of the assay.

3.3. Target detection in saliva and RNA as a target

The proof-of-principle experiments shown in Figs. 1 and 2 were performed in a well-defined buffer system using synthetic ssDNA as a target. To be functional as a point-of-need test for the detection of infectious diseases, however, the assay must also work under relevant biological conditions, preferentially with only very limited sample preparation required.

Especially for SARS-CoV-2-testing, saliva is emerging as an easy-to-collect and reliable testing species. To test the feasibility of MPS-based diagnostics as a viable tool for point-of-need testing, MPS measurements were performed in freshly collected, heat-inactivated saliva spiked with target DNA (Fig. 3A).

To this end, saliva was heated to 95 °C for 30 min before adding concentrated TE-buffer (pH of 7.4), $MgCl_2$ and ssDNA target to a concentration of 22.2 nM. Similar to using TE-based buffer as the assay medium, a decrease of the harmonic ratio upon target-binding is observable (Fig. 3A, black and blue curve, respectively). Since the viscosity of saliva is strongly dependent on external influences and varies from day to day and person to person, it is unavoidable to include a control sample. In this case, a saliva sample spiked with non-matching DNA was used. The resulting harmonic ratio spectrum (red) is very similar to the control without any target DNA (black), indicating that the observed decrease in harmonic ratio is caused by the specific crosslinking of MNPs and PS beads mediated by the matching target DNA.

In a real-world assay, unmodified MNPs or MNPs modified with an arbitrary, non-matching sequence can be used as a control to account for

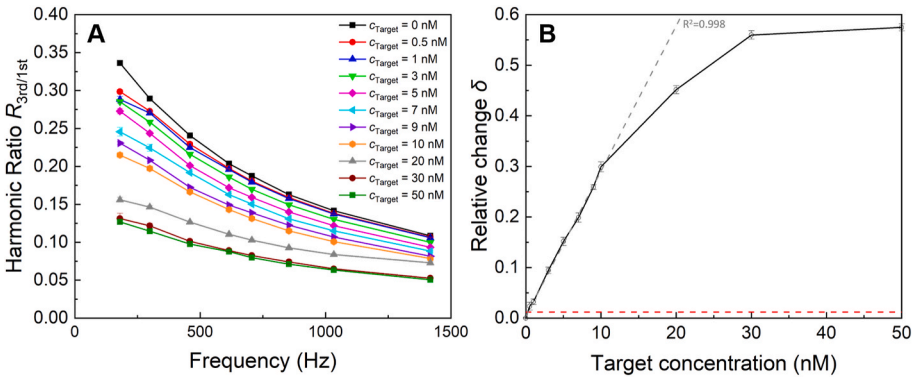

Fig. 2. *Influence of target concentration. A: The harmonic ratio decreases upon addition of target DNA in different concentrations. B: The relative change δ, being the difference between the measured harmonic ratio in presence of the target and the blank probe (c=0) normalized by the harmonic ratio of the blank probe, against target concentrations measured at* 459 Hz. *A linear range up to* 10 nM *target concentration is observable (grey line). For higher target concentrations, this linear behaviour is no longer valid, which can be explained by a saturation effect. Red line: limit of detection calculated by 3σ criterion being 0.*28 nM. *(For interpretation of the references to color in this figure legend, the reader is referred to the Web version of this article.)*

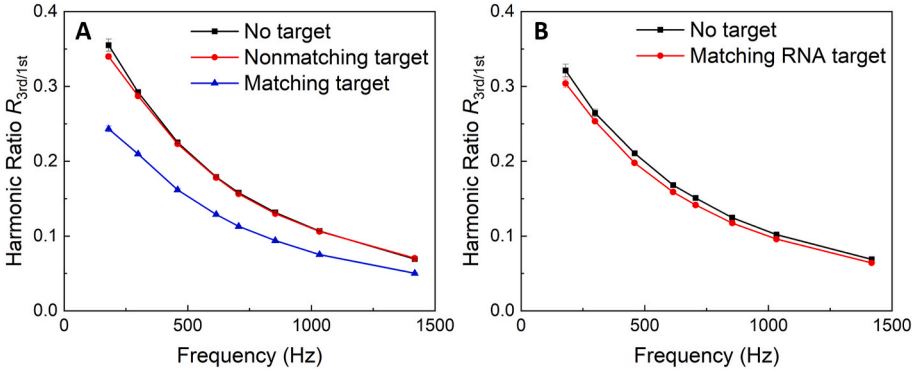

Fig. 3. Assays in relevant biological conditions. A: Using freshly collected heat-inactivated saliva as a sample medium, a specific change in the harmonic ratio upon addition of target DNA is observed (blue) compared to no (black) or nonspecific (red) target. B: Using RNA as a target (red), a decrease in the harmonic ratio compared to a control sample without target (black) is observable. (For interpretation of the references to color in this figure legend, the reader is referred to the Web version of this article.)

the individual viscosity of saliva.

In addition to saliva as a sample medium, we successfully used extraction buffer employed in commercially available SARS-CoV-2-tests enriched with target DNA (see Fig. S4)

Covid-19 is caused by an RNA-virus, therefore a direct detection of RNA would eliminate the need of further sample processing and enzymatic reactions. Since RNA can also hybridize with single-stranded DNA to form an RNA-DNA-duplex, similarly to Fig. 1A crosslinking of DNA-modified particles by the matching RNA target is expected. As shown in Fig. 3B, the addition of single-stranded 20A20C-RNA target to a solution of MNPs and PS beads modified with ss 20T and 20G DNA, respectively, changes the harmonics spectrum received similarly to using DNA as a target. The less-pronounced decrease when using RNA compared to DNA as a target under identical conditions (see Fig. S5) can be explained by the lower melting temperature of DNA-RNA-hybrids, eventually leading to less pronounced crosslinking, and to RNA degradation over time. To circumvent RNA degradation, RNase-free buffers were used and samples were kept on ice whenever possible. Interestingly, the RNA-mediated hybridized cluster were stable at room temperature over several days, resulting in similar spectra (data not shown).

3.4. Detection of a SARS-CoV-2-specific target

Besides using a PS bead mediated crosslinking of MNPs, also a more direct detection strategy using only MNPs can be envisioned: In the simplest case, the hybridization of target nucleic acid to MNPs carrying the complementary sequence leads to a change in hydrodynamic radius sufficient for detection via MPS. The effect under the current conditions was observable, albeit very weak and target-dependent (data not shown), therefore we extended the experiment to using two batches of modified MNPs carrying each a specific modification, both complementary to different parts of the target to be detected. By this direct crosslinking of MNPs, a similar effect as shown before is expected, eventually increasing the sensitivity due to the need of lower particle concentration.

To demonstrate the feasibility of this approach for the detection of relevant nucleic acid sequences, the random DNA-sequences used beforehand were changed based on currently used sequences for the detection of SARS-CoV-2 via RT-PCR.

Based on established PCR-testing sequences for the N-gene of SARS-CoV-2-virus (Corman et al., 2020), sequences were chosen based on forward and reverse primer as well as the probe, to modify streptavidin-coated MNPs via biotin-streptavidin interaction (see Table 1). As a target, complementary synthetic ssDNA was used. In contrast to the artificial target sequence 20A20C with according MNP-modification, the hybridization in this case is more demanding: A 20A-20T-hybridization can temporarily also only partially hybridize (leaving sticky ends) if a full hybridization is hindered due to steric or kinetic reasons. For these specific sequences, full hybridization is required. Furthermore, ssDNA structures tend to form sequence-specific secondary and tertiary structures which can hinder hybridization processes. Table S7 shows calculated structures as well as corresponding free energies of these sequences (SantaLucia, 1998; Zuker, 2003).

To test the feasibility of the assay, we therefore designed a set of three experiments A, B and C based on these three sequences, each containing two out of the three sequences to modify MNPs and the respective target (Table 1). In this case, the target-mediated crosslinking of MNPs was chosen as the base for change of the hydrodynamic radius. Therefore, for each experiment, two batches of MNPs were modified with the respective ssDNA-sequence. These two batches were then mixed and incubated with the respective target.

As can be seen in Fig. 4, in all three experiments a substantial increase in the hydrodynamic radius of the MNPs is observable as indicated by the reduction of harmonic ratio by more than 25 % for all tested sequences. In contrast, when incubating with a non-matching target (red curves), no decrease in the harmonic ratio is observed.

From this we conclude that the assay principle is suitable also for specific nucleic acid sequences as needed for example for the detection of SARS-CoV-2.

3.5. Improving the limit of detection

For an assay compatible with the demands of point-of-need testing, one of the most important characteristics is its sensitivity. In the primary experiments done so far, high concentrations of target nucleic acids in the nanomolar regime were used, showing the feasibility of the principle. However, for most cases a working range which is substantially lower is required.

Since there are a lot of parameters determining the sensitivity of this assay type, optimizing these set screws is a complex problem with many factors influencing each other and is therefore beyond the scope of this paper. To point the way to go, we chose several parameters individually, each of them affecting the performance of the test (see Fig. 5).

As there is no purification step after binding of biotinylated ssDNA to streptavidin-coated MNPs or PS beads, unbound ssDNA will remain in the sample. These strands will compete for target binding, probably being more efficient in hybridization due to a higher mobility. To eliminate this unwanted secondary reaction, a purification step can be added: We compared an unpurified sample as used in the measurements before to a sample where after the modification of the particles a filtering step using centrifugal filters was added. To this end, MNPs modified with 20T and PS beads modified with 20G were washed in amicon centrifugal tubes via centrifugation. Fig. 5A shows a comparison between these two methods for different target (20A20C) concentrations. The target-mediated relative change δ is substantially bigger for the purified sample (light colors) both for high (red) and low (black) concentration. Extrapolation of the data suggests that by this method, also detection of target concentrations in the picomolar range is feasible.

Compared to unwashed samples, MNPs washed in this way show a slightly modified behaviour in the magnetic field, which is probably due

Table 1
sequences used for the specific detection of SARS-CoV-2.

	Modification on MNP1	Modification on MNP2	target	mismatched target
A	GATTGCGGGTGCCAATGTG	GAGGAACGAGAAGAGGCTTG	CACATTGGCACCCGCAATCCAAGCCTCTTCTCGTTCCTC	CACATTGGCACCCGCAATCCAAGCCTCTTCTCAAGGAACAACATTGCCA
B	GATTGCGGGTGCCAATGTG	TGGCAATGTTGTTCCTTGAGGAAGT	CACATTGGCACCCGCAATCACTTCCTCAAGGAACAACATTGCCA	ACTTCCTCAAGGAACAACATTGCCACAAGGCTCTTCTCGTTCCTC
C	TGGCAATGTTGTTCCTTGAGGAAGT	GAGGAACGAGAAGAGGCTTG	ACTTCCTCAAGGAACAACATTGCCACAAGCCTCTTCTCGTTCCTC	CACATTGGCACCCGCAATCCAAGCCTCTTCTCGTTCCTC

to a change in particle size distribution in the filtering process (data now shown). Due to the control measurement without target, however, this can be taken into account. The downside of this filtering process is the loss of particles (data not shown). This explains the bigger standard deviations indicated and can be improved by using higher concentrated solutions.

Both MNPs and PS beads modified with ssDNA are stable for several weeks at 4 °C (see Fig. S3): MPS measurements show a very similar spectrum for freshly prepared particles and particles modified and kept in the fridge for up to 9 weeks before target addition. This means that for a point-of-need test, the local sample preparation can be minimized since the time-consuming incubation of the particles with biotinylated ssDNA and the filtering-process can be done beforehand.

Another possibility to reach lower concentration detection is to concentrate the MNP-target-crosslinks prior to measurement. Since the target binds to magnetic nanoparticles, magnetic concentration procedures can be used. Due to the small size of the MNPs, strong magnetic field gradients are needed for an efficient separation. MACS (Magnetic Activated Cell Sorting) columns contain a matrix composed of iron spheres, which convert an external magnetic field to strong field gradients, which then are sufficient to efficiently bind the MNPs used here. Upon removal of the external field, MNPs can be recovered in a high concentration. Therefore, MACS columns were used to concentrate the MNPs after incubation with a solution of target in different concentrations. As can be seen in Fig. 5B, for all target concentrations down to 0.5 nM (black, red and blue curve) δ is approximately 0.4, showing the applicability of this method for the detection of low-concentrated target.

In comparison to a solution of MNPs that were not subjected to MACS filtering, however, also the control sample without target exhibits an (albeit smaller) shift of harmonic ratio (data not shown). This is probably due to an enrichment of certain particle sizes due to the magnetic separation process and can be taken into account by an appropriate control measurement. Similar to amicon filtering, also in this process a substantial amount of particles is lost (data now shown), calling for further improvement of the process.

Other crucial parameters are the concentration of MNPs and their proportion to the (expected) target concentration: For a reliable signal, the current setup is run with a concentration of MNPs between 1 nM and 2 nM. Furthermore, the detection scheme can influence data quality, in particular whether using direct crosslinking of the MNPs carrying two different ssDNA sequences or using modified PS beads for crosslinking. To this end, we designed a set of experiments systematically varying the concentration of MNPs and target for both detection strategies. The particles were modified with 20T and 20G, respectively, using 20A20C as a target. The deviation factor δ at 299 Hz excitation frequency in dependence of the target concentration is shown both for direct MNP-crosslinking (black, blue and red) and PS bead-mediated crosslinking (green, pink, cyan) in Fig. 5C. As can be seen for low MNP concentrations, a target-concentration dependent saturation takes place, lowering δ for higher target concentration (black, red and green curves), making the assay less sensitive. This can be explained by a (partial) saturation of the ssDNA-modified MNPs and PS beads by the target, meaning that further crosslinking is impeded as also shown in Fig. 2.

Interestingly, in the experiments based on direct crosslinking of the MNPs the saturation takes place at lower target concentrations and already for a BNF concentration of 1 nM (black), whereas the PS bead mediated binding shows saturation only at a lower BNF-concentration of 0.5 nM (green). This is in congruence with the total binding capacity in the sample: Assuming a similar binding capacity of modified PS beads and MNPs, the binding capacity in the experiments using PS beads is approximately doubled compared to direct MNP crosslinking. In the direct crosslinking experiments, both binding partners (carrying 20T and the 20G sequence, respectively) are MNPs, therefore both are contributing to the total BNF concentration. For the PS bead mediated binding, all MNPs are modified with 20G, whereas the PS beads carry the 20T sequence. For identical total BNF concentration and a 1:1 ratio

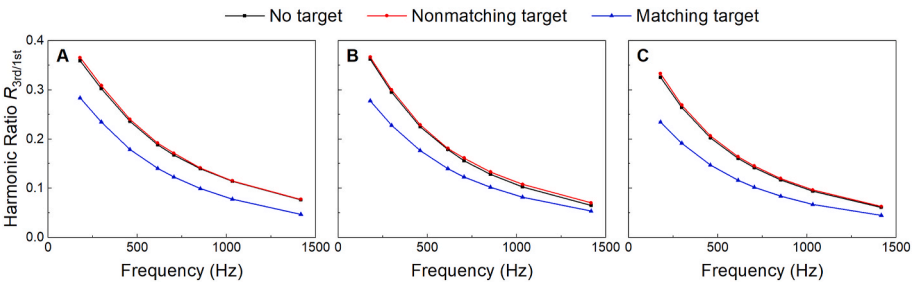

Fig. 4. Detection of SARS-CoV-2-related specific DNA sequences. MNPs were modified with two different sequences derived from the N-gene of SARS-CoV-2. Upon addition of target DNA consisting of complementary parts (blue), a change in harmonic ratio for all measured frequencies is visible compared to no or non-matching targets (red and blue) for all tested sequences. In this case, the target-mediated crosslinking of differently modified MNPs was used. (For interpretation of the references to color in this figure legend, the reader is referred to the Web version of this article.)

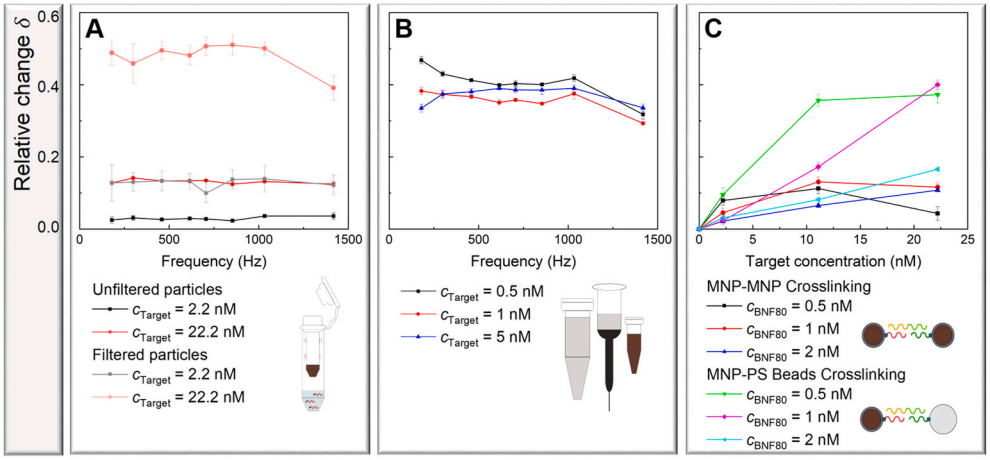

Fig. 5. *Factors determining the detection limit. For a better overview, instead of showing the harmonic ratio for sample and control measurements, the relative change in harmonics δ is shown. The closer δ is to 1, the stronger the change in MPS signal upon target-mediated binding. A: When using amicon filters to remove unbound ssDNA from the particle solution, in the purified sample (light colors) the same target concentrations (2 nM and 22 nM, respectively), give rise to a larger relative change δ compared to a non-purified sample (dark colors). The increase in error bars is due to a loss in nanoparticles in the purification process, which results in a weaker signal with higher deviation. B: Upconcentration of a larger volume containing MNPs and different amounts of target DNA using Magnetic Activated Cell Sorting (MACS) columns. For all concentrations down to 500 pM, a substantial relative change δ is visible. C: Comparison of target-mediated crosslinking of MNPs with PS beads (cyan, purple and green) to target-mediated crosslinking of MNPs carrying two different DNA sequences (black, red and blue). Different concentrations of MNPs and PS beads as well as target DNA were chosen and the respective relative change in harmonic ratio was plotted against the different target concentrations. For low MNP concentrations, a saturation effect is observable in the respective target concentration range (black, green and partially red). (For interpretation of the references to color in this figure legend, the reader is referred to the Web version of this article.)*

of PS beads and MNPs in the latter case, the binding capacity is approximately doubled, resulting in the onset of saturation effects at roughly double the target concentration or half the BNF concentration.

For lower target concentrations, however, a lower MN

P concentration gives rise to a stronger deviation. Comparing the detection strategies, from these data the approach of using PS beads for crosslinking MNPs seems to be advantageous for low target concentrations, showing a bigger deviation factor δ.

4. Conclusion

In recent years, MPS was established as a valuable tool for characterizing the behaviour of magnetic particles.

Here we demonstrate the application of MPS to detect specific nucleic acid sequences as needed for precise and sensitive diagnostic assays. On the basis of nucleic acid-mediated changes in hydrodynamic radius, a simplified detection of pathogens like SARS-CoV-2 becomes feasible. Since both DNA and RNA were successfully detected using MPS and also saliva as a biologically relevant test specimen does not hamper the detection, a wide variety of diagnostic applications are conceivable.

It was shown that the LoD, which was estimated to be 0.28 nM, can be improved by filtering, magnetic upconcentration and changes in MNP concentration. By further improvements of the assay, detection of low concentrated targets in the low pico- or even femtomolar regime without the need of further molecular amplification or sample processing comes into reach, matching the needs of rapid saliva-based diagnostics.

Important points here include the optimization of size and magnetic characteristics of the MNPs, the density of particle functionalization and the washing procedure of functionalized particles, improvements in the kinetics of the crosslinking reaction for example by active magnetic mixing and tailoring the sequences for optimized binding, eventually including spacers for lowering steric hindrance of the binding reaction. On the other hand, we are engineering an improved setup with higher sensitivity due to an optimized design which will be used for further improvements of the assay. For even higher demands, this approach can be augmented in a modular way by further sample processing steps like well-established (enzymatic) multiplication of the target.

Compared to well-established diagnostic assays based on luminescence, electrochemistry or colorimetry, our magnetism-based approach stands out due to the inherent possibility to exploit one-step magnetic sample purification, allowing for an easy and rapid diagnostic workflow. Furthermore, opaque sample media can be used without increasing background level, contributing to fast and cost-efficient sample processing.

Due to the ubiquity of nucleic acid hybridization and the ease of adapting the test to new sequences, we expect this approach to be feasible in a wide regime of possible applications, including quantitative diagnostics of novel pathogens, screening for mutations like the increasingly important variants of SARS-CoV-2 or personalized medicine.

Taken together, these results will pave the way for the development of a rapid, cost-efficient, sensitive and reliable point-of-need diagnostic platform based on magnetic particle spectroscopy for the detection of pathogen-specific nucleic acids.

Funding

This work was supported by the Deutsche Forschungsgemeinschaft (DFG, German Research Foundation) under Germany's Excellence Strategy – EXC-2123 QuantumFrontiers – 390837967, the DFG Research Training Group 1952 Metrology for Complex Nanosystems, ZH 782/1-1 and "Niedersächsisches Vorab" through "Quantum- and Nano-Metrology (QUANOMET)" initiative within the projects NL-1 (BL) and NL-2 (TV).

CRediT authorship contribution statement

Enja Laureen Rösch: Investigation, Validation, and, Visualization. **Jing Zhong:** Resources, and, Formal analysis. **Aidin Lak:** Validation. **Zhe Liu:** Investigation, and, Validation. **Markus Etzkorn:** Validation. **Meinhard Schilling:** Supervision. **Frank Ludwig:** Methodology. **Thilo Viereck:** Conceptualization, Methodology, and Writing. **Birka Lalkens:** Conceptualization, Methodology, Investigation, Supervision, and Writing. All authors contribute to discussion and writing.

Declaration of competing interest

The authors declare that they have no known competing financial interests or personal relationships that could have appeared to influence the work reported in this paper.

Acknowledgement

Funding: This work was supported by the Deutsche Forschungsgemeinschaft (DFG, German Research Foundation) under Germany's Excellence Strategy – EXC-2123 QuantumFrontiers – 390837967, the DFG Research Training Group 1952 Metrology for Complex Nanosystems, ZH 782/1-1 and "Niedersächsisches Vorab" through "Quantum- and Nano-Metrology (QUANOMET)" initiative within the projects NL-1 (BL) and NL-2 (TV).

We thank Christian Köhn for help with DLS measurements.

Appendix A. Supplementary data

Supplementary data to this article can be found online at https://doi.org/10.1016/j.bios.2021.113536.

References

Afzal, A., 2020. J. Adv. Res. 26, 149–159.
Ahrentorp, F., Astalan, A., Blomgren, J., Jonasson, C., Wetterskog, E., Svedlindh, P., Lak, A., Ludwig, F., van IJzendoorn, L.J., Westphal, F., Grüttner, C., Gehrke, N., Gustafsson, S., Olsson, E., Johansson, C., 2015. J. Magn. Magn Mater. 380, 221–226. https://www.sciencedirect.com/science/article/pii/S0304885314008920.
Armbruster, D.A., Pry, T., 2008. Clin. Biochem. Rev. 29 (Suppl. 1), S49–S52.
Arnaout, R., Lee, R.A., Lee, G.R., Callahan, C., Yen, C.F., Smith, K.P., Arora, R., Kirby, J. E., 2020. bioRxiv.
Azzi, L., Carcano, G., Gianfagna, F., Grossi, P., Gasperina, D.D., Genoni, A., Fasano, M., Sessa, F., Tettamanti, L., Carinci, F., Maurino, V., Rossi, A., Tagliabue, A., Baj, A., 2020. J. Infect. 81 (1), e45–e50.
Biederer, S., Knopp, T., Sattel, T.F., Lüdtke-Buzug, K., Gleich, B., Weizenecker, J., Borgert, J., Buzug, T.M., 2009. J. Phys. D Appl. Phys. 42 (20), 205007. https://iopscience.iop.org/article/10.1088/0022-3727/42/20/205007/meta.
Corman, V.M., Landt, O., Kaiser, M., Molenkamp, R., Meijer, A., Chu, D.K.W., Bleicker, T., Brünink, S., Schneider, J., Schmidt, M.L., Mulders, D.G., Haagmans, B. L., van der Veer, B., van den Brink, S., Wijsman, L., Goderski, G., Romette, J.-L., Ellis, J., Zambon, M., Peiris, M., Goossens, H., Reusken, C., Koopmans, M.P.G., Drosten, C., 2020. Euro Surveill. 25 (3).
Draack, S., Lucht, N., Remmer, H., Martens, M., Fischer, B., Schilling, M., Ludwig, F., Viereck, T., 2019a. J. Phys. Chem. C 123 (11), 6787–6801.
Draack, S., Viereck, T., Nording, F., Janssen, K.-J., Schilling, M., Ludwig, F., 2019b. J. Magn. Magn Mater. 474, 570–573. https://www.sciencedirect.com/science/article/pii/S0304885318319474.
Fozouni, P., Son, S., Díaz de León Derby, M., Knott, G.J., Gray, C.N., D'Ambrosio, M.V., Zhao, C., Switz, N.A., Kumar, G.R., Stephens, S.I., Boehm, D., Tsou, C.-L., Shu, J., Bhuiya, A., Armstrong, M., Harris, A., Osterloh, J.M., Meyer-Franke, A., Langelier, C., Pollard, K.S., Crawford, E.D., Puschnik, A.S., Phelps, M., Kistler, A., DeRisi, J.L., Doudna, J.A., Fletcher, D.A., Ott, M., 2020. Direct Detection of SARS-CoV-2 Using CRISPR-Cas13a and a Mobile Phone.
Guglielmi, G., 2020. Nature 583 (7817), 506–509.
Haug, N., Geyrhofer, L., Londei, A., Dervic, E., Desvars-Larrive, A., Loreto, V., Pinior, B., Thurner, S., Klimek, P., 2020. Nature human behaviour 4 (12), 1303–1312.
Islam, K.U., Iqbal, J., 2020. Front.Cell.. Infect. Microbiol. 10, 694. https://www.frontiersin.org/article/10.3389/fcimb.2020.560616.
Kahmann, T., Ludwig, F., 2020. J. Appl. Phys. 127 (23), 233901.
Kevadiya, Bhavesh D., Machhi, Jatin, Herskovitz, Jonathan, Oleynikov, Maxim D., Blomberg, Wilson R., Bajwa, Neha, Soni, Dhruvkumar, Das, Srijanee, Hasan, Mahmudul, Patel, Milankumar, Senan, Ahmed M., Gorantla, Santhi, McMillan, JoEllyn, Benson, Edagwa, Eisenberg, Robert, Gurumurthy, Channabasavaiah B., Reid, St Patrick M., Punyadeera, Chamindie, Chang, Linda, Gendelman, Howard E., 2021a. Nat. Mater. 20 (5), 593–605. https://www.nature.com/articles/s41563-020-00906-z.
Kevadiya, B.D., Machhi, J., Herskovitz, J., Oleynikov, M.D., Blomberg, W.R., Bajwa, N., Soni, D., Das, S., Hasan, M., Patel, M., Senan, A.M., Gorantla, S., McMillan, J., Edagwa, B., Eisenberg, R., Gurumurthy, C.B., Reid, S.P.M., Punyadeera, C., Chang, L., Gendelman, H.E., 2021b. Nat. Mater. 1–13. https://www.nature.com/articles/s41563-020-00906-z#citeas.
Khurshid, H., Friedman, B., Berwin, B., Shi, Y., Ness, D.B., Weaver, J.B., 2017. AIP Adv. 7 (5), 56723.
Morales-Narváez, E., Dincer, C., 2020. Biosens. Bioelectron. 163, 112274. http://www.sciencedirect.com/science/article/pii/S0956566320302694.
Oliveira, B.A., Oliveira, L.C. de, Sabino, E.C., Okay, T.S., 2020. Revista do Instituto de Medicina Tropical de Sao Paulo, p. e44.
Park, C., Lee, J., Hassan, Z.u., Ku, K.B., Kim, S.J., Kim, H.G., Park, E.C., Park, G.-S., Park, D., Baek, S.-H., Park, D., Lee, J., Jeon, S., Kim, S., Lee, C.-S., Yoo, H.M., Kim, S., 2020. Robust and Sensitive Detection of SARS-CoV-2 Using PCR Based Methods.
Poller, W.C., Löwa, N., Wiekhorst, F., Taupitz, M., Wagner, S., Möller, K., Baumann, G., Stangl, V., Trahms, L., Ludwig, A., 2016. J. Biomed. Nanotechnol. 12 (2), 337–346.
Rauwerdink, A.M., Weaver, J.B., 2010. Appl. Phys. Lett. 96 (3), 33702.
Ravi, N., Cortade, D.L., Ng, E., Wang, S.X., 2020. Biosens. Bioelectron. 165, 112454.
SantaLucia, J., 1998. Proc. Natl. Acad. Sci. U. S. A 95 (4), 1460–1465.
Schrittwieser, S., Pelaz, B., Parak, W.J., Lentijo-Mozo, S., Soulantica, K., Dieckhoff, J., Ludwig, F., Guenther, A., Tschöpe, A., Schotter, J., 2016. Sensors 16 (6).
Tian, B., Han, Y., Wetterskog, E., Donolato, M., Hansen, M.F., Svedlindh, P., Strömberg, M., 2018. ACS Sens. 3 (9), 1884–1891.
Tian, B., Gao, F., Fock, J., Dufva, M., Hansen, M.F., 2020. Biosens. Bioelectron. 165, 112356. https://www.sciencedirect.com/science/article/pii/S095656632030350X.
Vandenberg, O., Martiny, D., Rochas, O., van Belkum, A., Kozlakidis, Z., 2021. Nat. Rev. Microbiol. 18, 171–183.
Wawrzik, T., Schilling, M., Ludwig, F., 2012. Perspectives of magnetic particle spectroscopy for magnetic nanoparticle characterization. In: Buzug, T.M., Borgert, J. (Eds.), Magnetic Particle Imaging. Springer Berlin Heidelberg, Berlin, Heidelberg, pp. 41–45.
Wu, K., Su, D., Saha, R., Wong, D., Wang, J.-P., 2019. J. Phys. D Appl. Phys. 52 (17), 173001.
Wu, K., Liu, J., Saha, R., Su, D., Krishna, V.D., Cheeran, M.C.-J., Wang, J.-P., 2020a. ACS Appl. Mater. Interfaces 12 (12), 13686–13697.
Wu, K., Su, D., Saha, R., Liu, J., Chugh, V.K., Wang, J.-P., 2020b. ACS Appl. Nano Mater. 3 (6), 4972–4989.
Zhong, J., Schilling, M., Ludwig, F., 2018. Meas. Sci. Technol. 29 (11), 115903.
Zhong, J., Janssen, K.-J., Draack, S., Viereck, T., Schilling, M., Ludwig, F., 2021a. J. Magn. Magn Mater. 517, 167408.
Zhong, J., Rösch, E.L., Viereck, T., Schilling, M., Ludwig, F., 2021b. ACS Sensors.
Zhou, Y., Pei, F., Ji, M., Wang, L., Zhao, H., Li, H., Yang, W., Wang, Q., Zhao, Q., Wang, Y., 2020. PloS One 15 (11), e0241469.
Zhu, J., Guo, J., Xu, Y., Chen, X., 2020. J. Infect. 81 (3), e48–e50.
Zuker, M., 2003. Nucleic Acids Res. 31 (13), 3406–3415.